

Caustics in turbulent aerosols

M. WILKINSON¹ and B. MEHLIG²

¹ *Faculty of Mathematics and Computing, The Open University, Walton Hall, Milton Keynes, MK7 6AA, England*

² *Theoretical Physics, Physics and Engineering Physics, Gothenburg University/Chalmers, Gothenburg, Sweden*

PACS. 05.40.-a – Random processes.

PACS. 47.27.Qb – Turbulent diffusion.

PACS. 47.54.+r – Pattern formation (fluid mechanics).

Abstract. – Networks of caustics can occur in the distribution of particles suspended in a randomly moving gas. These can facilitate coagulation of particles by bringing them into close proximity, even in cases where the trajectories do not coalesce. The long-time morphology of these caustic patterns depends upon the Lyapunov exponents λ_1 , λ_2 of the suspended particles, as well as the rate J at which particles encounter caustics. We develop a theory determining the quantities J , λ_1 , λ_2 from the statistical properties of the gas flow, in the limit of short correlation times.

Aerosols are usually unstable systems, in that the suspended particles eventually coagulate. Understanding the process giving rise to this coagulation, and determining the time scale over which it occurs are important questions in describing any aerosol system. If the gas phase does not have macroscopic motion, the coagulation may be effected by diffusion of the suspended particles, or (if the suspended particles are of a volatile substance) by Ostwald ripening. The coagulation process can be greatly accelerated if the aerosol undergoes macroscopic internal motion. Ultrasound, for example, has been used to accelerate coagulation in aerosols [1]. Turbulent flow could also play a role in the coagulation of suspended particles; this could be relevant in the coalescence of visible moisture into rain droplets [2].

If suspended particles are simply advected in an incompressible flow, their density remains constant. Inertial effects are therefore required for coagulation, unless the flow exhibits significant compressibility. In earlier work [3, 4] we discussed the motion of inertial particles in a random velocity field. We showed that there is a phase where the trajectories of the particles coalesce, so that arbitrarily small particles coagulate. In the limit where the correlation time τ of the flow approaches zero, this path-coalescing phase only exists when the velocity field is predominantly potential flow (such as the flow due to sound waves) [4].

Turbulent fluid flow is, however, expected to be predominantly solenoidal, and it is of interest to find alternative mechanisms of coagulation which operate outside the path-coalescence phase. Here we describe an alternative mechanism facilitating coagulation, illustrated in Fig. 1: we show the distribution of particles suspended in a randomly moving gas (the equations of motion and statistics of the flow field are given by eqns. (1) to (3) below). The large

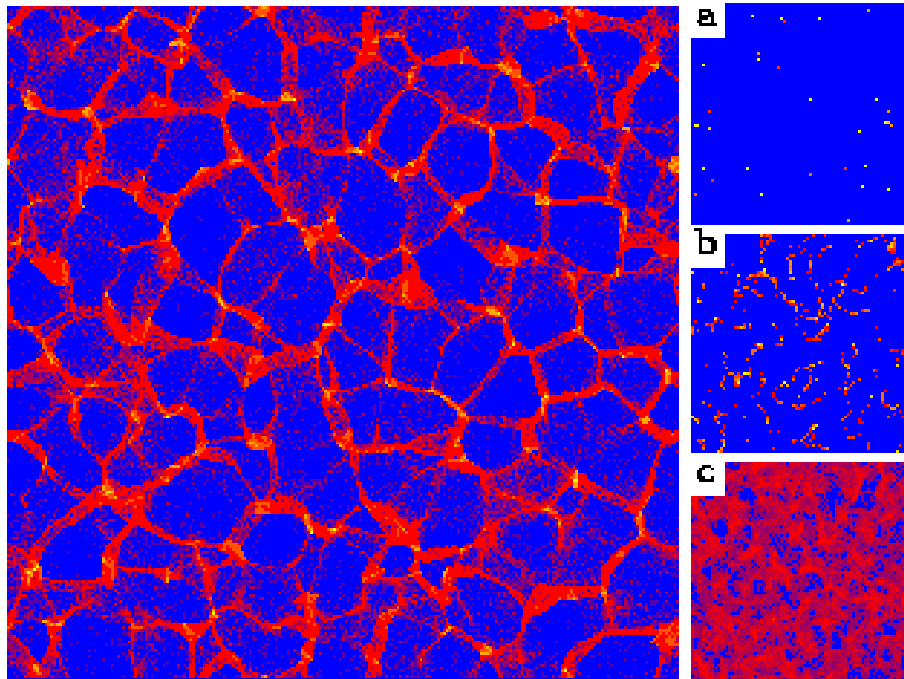


Fig. 1 – Distribution of inertial particles suspended in a randomly moving fluid (blue corresponds to lowest density, yellow to highest). The initial distribution is a random scatter. The large panel shows caustics at short time. Panels (a)-(c) show the long-time behaviour. In all cases, the region is the unit square, the mean particle density is 2.5×10^5 , $m = 1$, and there is potential flow (with parameters $\xi = 0.03$, $\sigma = 0.01$, $\delta t = 0.05$, see text). Main panel: $\gamma = 0.53$, $t = 5$, (a): $\gamma = 1.18$, $t = 500$, (b): $\gamma = 0.72$, $t = 125$, (c): $\gamma = 0.21$, $t = 125$. The three cases correspond to: (a) $\lambda_2 < \lambda_1 < 0$, (b) $\lambda_1 > 0$, $\lambda_1 + \lambda_2 < 0$, and (c) $\lambda_1 > 0$, $\lambda_1 + \lambda_2 > 0$, see text.

panel shows the distribution of particles after a short time, starting from a random scatter with uniform density. The particles cluster onto a network of caustic lines, analogous to the networks of optical caustics that can be seen on the bottom of a swimming pool [5]. This phenomenon is a new mechanism by which aerosol particles are brought into close proximity. The remaining parts of Fig. 1 show the distribution of particles after a long time, in three different cases: part (a) shows the path-coalescence phase where the trajectories condense onto points. Parts (b) and (c) show two cases where there is no path coalescence, but a steady state with significant inhomogeneities of density due to caustics: these have very different morphologies, depending on the parameter values, as we shall show.

Fig. 1 is surprising because it is expected that random movement of uniformly distributed particles would leave the distribution uniform. The following questions naturally arise. First, why do the particle trajectories coalesce into points in Fig. 1(a)? This phenomenon was first noted in [6] and subsequently analysed in detail in [3, 4] (c.f. also the theory developed at the end of this paper). Secondly, why and how does the caustic pattern develop? We will explain why the caustics form, and relate the pattern to optical caustic networks in swimming pools. Third, why do the morphologies of the structures seen in the steady state at long times differ? We will argue that the different morphologies of the caustic patterns are related to three parameters: the rate J at which any given particle crosses a

caustic and the Lyapunov exponents λ_1 and λ_2 of the flow (with $\lambda_1 > \lambda_2$). We present a new theory for these parameters in the limit where the correlation time of the random flow is short. Finally, it is natural to ask how the density fluctuations are quantified. We will show that the probability distribution function for the particle density has two regimes of algebraic decay. The formation of caustics causes particles to pass through regions of greatly increased density, where coagulation by contact interaction is much more likely to occur. In this paper we confine ourselves to describing the caustics, and do not model the coagulation process.

There is a large literature on light-intensity fluctuations in twinkling starlight, and other cases of propagation through random media. Such problems are different because the finite wavelength of the light causes the fluctuation distribution due to catastrophes to be cutoff at high intensities [5]. Caustics also occur in Hamiltonian dynamics, and their observation in electron flows is a topic of current research [7], where the statistics of caustic formation are of interest [8]. Our system differs from the Hamiltonian case: the drag force on the particles is assumed to be given by Stokes's law. Because of the Stokes damping, the density correlation function reaches a statistically stationary state, as opposed to the Hamiltonian case. Although our results are described in the context of aerosols, the same principles apply to suspensions of particles in liquids and to tracer particles used to investigate turbulent flows. Because our objective is to explain the theoretical principles as clearly as possible, we confine discussion to one or two spatial dimensions.

We consider small spherical non-interacting particles of mass m , radius a , in a random flow with velocity field $\mathbf{u}(\mathbf{r}, t)$ and viscosity η . We assume that the drag force on the particles is given by Stokes's law. Neglecting displaced-mass effects, the equation of motion is

$$\ddot{\mathbf{r}} = -\gamma(\dot{\mathbf{r}} - \mathbf{u}) \quad (1)$$

where $\gamma = 6\pi\eta a/m$ and \mathbf{r} is the particle position. This model is widely used in studies of particles suspended in turbulent fluids (see [9], [10] for descriptions of recent numerical investigations of this model), and it is surprising that the occurrence of caustics was not noted earlier. The random driving force on the particles, $\mathbf{f} = m\gamma\mathbf{u}$, is conveniently described by two scalar potentials ϕ and ψ :

$$\mathbf{f}(\mathbf{r}, t) = \nabla\phi(\mathbf{r}, t) + \nabla \wedge \hat{\mathbf{n}}_3\psi(\mathbf{r}, t) \quad (2)$$

(where $\hat{\mathbf{n}}_3$ is a unit vector perpendicular to the plane): the scalar fields ϕ and ψ generate, respectively, the potential and solenoidal components of the flow. Here we assume that ϕ and ψ are independent, with $\langle\phi\rangle = \langle\psi\rangle = 0$ and $\langle\psi^2\rangle = \alpha^2\langle\phi^2\rangle$ for some constant α (angular brackets denote expectation values). Also, we assume that the correlation function of ψ has the same form as that of ϕ :

$$\langle\phi(\mathbf{r} + \mathbf{R}, t_0 + t)\phi(\mathbf{r}, t_0)\rangle = C(R, t), \quad (3)$$

where $R = |\mathbf{R}|$, and $C(R, t)$ has correlation length ξ and correlation time τ . The theory is readily extended to more general statistics.

Our two-dimensional numerical simulations are performed in the limit of small τ , using a model discretised in time with a small time step $\delta t \gg \tau$: the impulse

$$\mathbf{f}_n(\mathbf{r}) = \int_{n\delta t}^{(n+1)\delta t} dt' \mathbf{f}(\mathbf{r}_{t'}, t') \quad (4)$$

at time $n\delta t$ is taken to be of the form (2) in terms of scalar fields $\phi_n(\mathbf{r})$ and $\psi_n(\mathbf{r})$ satisfying $\langle\phi_n(\mathbf{r})\phi_{n'}(\mathbf{r}')\rangle = \sigma^2 \xi^2 \delta t \exp(-|\mathbf{r} - \mathbf{r}'|^2/2\xi^2)\delta_{nn'}$ and $\langle\psi_n(\mathbf{r})\psi_{n'}(\mathbf{r}')\rangle = \alpha^2\langle\phi_n(\mathbf{r})\phi_{n'}(\mathbf{r}')\rangle$.

The origin of the caustics is most easily understood by a one-dimensional example. Fig. 2 (a) is a schematic plot of the momentum p of a particle at position x . At time $t = 0$, this is a single-valued function, but at a later time this function may develop a pair of folds because the faster particles overtake the slower ones. If the density of particles is smoothly distributed along the line in phase-space, the projected density in coordinate space, shown in part (b), is singular at a pair of caustics, which are the projections of each fold. We see that the caustics are created in pairs, and that initially there is a high density of particles between the caustic lines, as well as a divergent density on the caustic itself. Fig. 2 (c) shows a segment of the actual caustic pattern. The caustic lines cannot abruptly end, but caustics can join at cusps [5], some of which are visible in the figure. Some regions of high density do not have an associated pair of caustic lines. This is because the phase-space manifold is nearly perpendicular to the coordinate-space plane, but it has not yet folded over. At short times our caustic networks are equivalent to the lines of bright light observed on the bottom of a swimming pool on a sunny day when the water surface is disturbed. The morphology of the swimming-pool caustics is discussed by Berry [5].

There are important differences between optical realisations of caustic patterns behind randomly refracting screens and the caustics in particle density. The former become more confused as the distance from the screen is increased, whereas our patterns reach a statistically steady state at large times. Although more caustics are created by folding, the damping term (with coefficient γ in eq. (1)) implies that momentum differences decrease, so that the caustics become progressively more tightly folded.

The examples in Fig. 1(b) and (c) show that the morphology of the patterns in this steady state depends upon the statistics of the random velocity field. It is desirable to understand the differences between these figures.

We consider the behaviour of three particles, a reference particle and two nearby ones separated by $\delta\mathbf{r}$ and $\delta\mathbf{r}'$. The evolution of these small increments is described by the Lyapunov exponents, λ_1 and λ_2 , characterising the time-dependence of the length $X(t) = |\delta\mathbf{r}(t)|$ of one of the separation vectors, and of the area of a parallelogram spanned by two vectors,

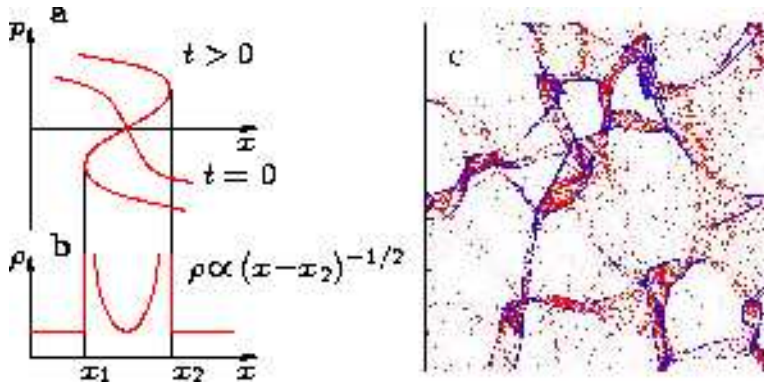


Fig. 2 – (a) Particles are distributed on a phase-space manifold, shown here as a phase curve in a one-dimensional section. The phase curve develops folds. (b) The particle density diverges on caustics, the projections of the folds. The caustics are created in pairs, with a high density of particles between each pair. (c) The particle distribution is shown in red, and the corresponding caustic curves are plotted as blue lines. The parameters are the same as for the largest panel of Fig. 1.

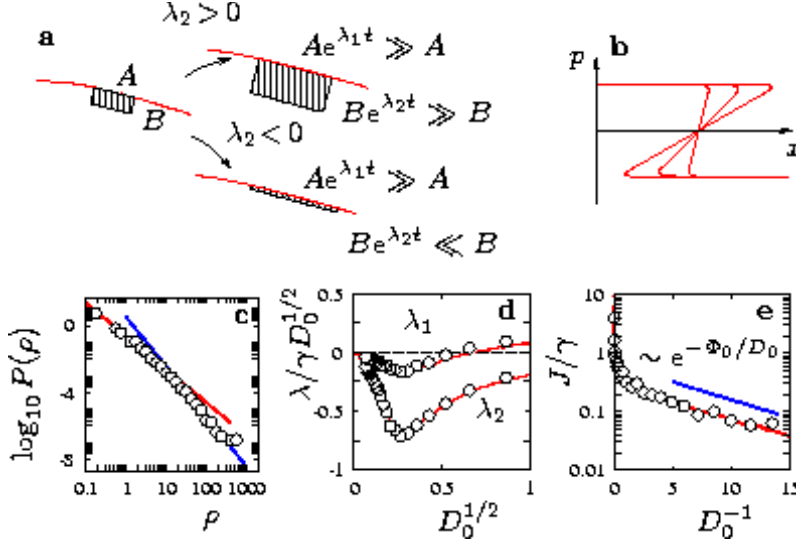


Fig. 3 – (a): The Lyapunov exponents λ_1 and λ_2 determine the particle-density fluctuations. (b): Schematic illustration of the model for the folding process leading to eq. (6). (c): Density fluctuations in a one-dimensional model ($\xi = 0.05$, $m = 1$, $\tau = 1$, $\sigma = 10^{-3}$, $\gamma = 0.04$, averaged over 25 times ranging from 40τ to $10^3\tau$): $P(\rho)$ shows algebraic decay, with a region of ρ^{-2} decay followed by a ρ^{-3} tail. (d): Lyapunov exponents λ_1 and λ_2 for $\Gamma = 1/3$; simulations of Langevin equations (lines) and integration of equation of motion (o). (e): Corresponding rate of crossing caustics.

$A(t) = |\delta \mathbf{r}(t) \wedge \delta \mathbf{r}'(t)|$. These are defined by

$$\lambda_1 = \lim_{t \rightarrow \infty} \frac{1}{t} \log_e \left| \frac{X(t)}{X(0)} \right|, \quad \lambda_1 + \lambda_2 = \lim_{t \rightarrow \infty} \frac{1}{t} \log_e \left| \frac{A(t)}{A(0)} \right|. \quad (5)$$

Now we use the Lyapunov exponents to gain an understanding of the patterns in Fig. 1. When $\lambda_1 < 0$, almost all infinitesimal line segments contract to a point, and the trajectories of particles coalesce as shown in Fig. 1(a). This was the principle used to explain the coalescence transition, discussed in [3] and [4]. Next consider what happens if λ_1 is positive, so that the trajectories do not coalesce into points. In this case we consider a small element of area on a caustic line, extended in the direction of the caustic [Fig. 3(a)]. This element is expected to be stretched along the direction of the caustic, because we assume $\lambda_1 > 0$. If λ_2 is also positive, the line width of the element will also expand in the direction perpendicular to the caustic, and the density fluctuation resulting from the caustic becomes weaker as time proceeds: this is illustrated by Fig. 1(c). If $\lambda_2 < 0$, the line element contracts in the direction perpendicular to the caustic, and if in addition $\lambda_1 + \lambda_2 < 0$, the concentration of particles on the caustic increases. This case is illustrated by Fig. 1(b), which shows very narrow caustic lines. The increase in particle density on the caustic lines cannot proceed without limit: the caustic line stretches and folds, until the particles aligned along the caustic have become indistinguishable from points randomly scattered in the plane. In this case, the caustic also disappears, although this happens much more slowly than when $\lambda_1 + \lambda_2 > 0$.

A useful quantitative understanding of the steady state can be gained by considering the probability distribution of the particle density, $P(\rho)$. The particle density in the vicinity of a caustic (at x_0 , aligned with the y axis, say) has a divergence of the form $\rho(x, y) \sim (x - x_0)^{-1/2}$.

This indicates that $P(\rho) \sim \rho^{-3}$ for sufficiently large ρ . However, numerical evaluations of $P(\rho)$ indicates that $P(\rho) \sim \rho^{-2}$ over a significant range of values, only conforming to the ρ^{-3} prediction for very large ρ . This surprising observation is a consequence of the nature of the folding process which generates the caustics, and we give a brief heuristic argument which illustrates the principle. Consider the schematic diagram in Fig. 3(b), which shows a simplified model for the evolution of a fold which forms at $t = 0$, with a depth which is proportional to time t . The corresponding density distribution at time t is $P(\rho, t) = tf(\rho t)$ for some function f . The pattern contains folds at different stages of their evolution, and the observed probability distribution function $P(\rho)$ is assumed to be a time-average of $P(\rho, t)$, between $t = 0$ and some cutoff t_0 (which can be interpreted as the time between the formation of folds). According to this model,

$$P(\rho) = \frac{1}{t_0} \int_0^{t_0} dt P(\rho, t) = \frac{1}{\rho^2 t_0} \int_0^{\rho t_0} dx xf(x) \sim \rho^{-2} \quad (6)$$

(we assume that the integral of $xf(x)$ converges to a constant as its upper limit approaches infinity). The model is not applicable at very short times, where the fold resembles the generic type illustrated in Fig. 2(a). Fig. 3(c) illustrates the crossover from ρ^{-2} to ρ^{-3} decay in a numerical evaluation of $P(\rho)$.

We have argued that the morphology of the steady state caustic patterns can be understood qualitatively if we calculate three parameters, namely the rate J at which particles cross caustic lines, and the Lyapunov exponents λ_1 and λ_2 . We will now show how these three parameters may be determined quantitatively. The most complete results are available in the limit where the correlation time τ is very short.

We linearise eq. (1), and obtain $\delta \dot{\mathbf{r}} = \delta \mathbf{p}/m$, $\delta \dot{\mathbf{p}} = -\gamma \delta \mathbf{p} + \mathbf{F}(t) \delta \mathbf{r}$, where \mathbf{F} is a matrix with elements $F_{ij}(t) = \partial f_i(\mathbf{r}(t), t) / \partial r_j$. Consider now the motion of three particles, one reference particle and two nearby ones, separated by $(\delta \mathbf{r}, \delta \mathbf{p})$ and $(\delta \mathbf{r}', \delta \mathbf{p}')$ from the reference trajectory. The angle $\delta \varphi$ separating the vectors $\delta \mathbf{r}$ and $\delta \mathbf{r}'$ is very small, and the lengths of these vectors, X and X' respectively, are initially equal. We also assume that the vectors $\delta \mathbf{p}$ and $\delta \mathbf{p}'$ are initially separated by a small angle, of order $\delta \varphi$. We now make a change of coordinates from $\delta \mathbf{r}, \delta \mathbf{p}, \delta \mathbf{r}', \delta \mathbf{p}'$ to the set $X, X', \theta, \delta \varphi, Y_1, Y_2, Z_1, Z_2$

$$\begin{aligned} \delta \mathbf{r} &= X \hat{\mathbf{n}}_\theta, & \delta \mathbf{r}' &= X' \hat{\mathbf{n}}_{\theta+\delta \varphi} \\ \delta \mathbf{p} &= X(Y_1 \hat{\mathbf{n}}_\theta + Y_2 \hat{\mathbf{n}}_{\theta+\pi/2}), & \delta \mathbf{p}' &= X'[(Y_1 + Z_1 \delta \varphi) \hat{\mathbf{n}}_{\theta+\delta \varphi} + (Y_2 + Z_2 \delta \varphi) \hat{\mathbf{n}}_{\theta+\frac{\pi}{2}+\delta \varphi}] \end{aligned} \quad (7)$$

($\hat{\mathbf{n}}_\theta$ denotes a unit vector in two dimensions with direction θ). We expect that X may increase or decrease, $\delta \varphi$ decreases with probability one (because random linear mapping of any two vectors results in vectors becoming aligned), X'/X remains close to unity, θ will become uniformly distributed on $[0, 2\pi]$, and that Y_1, Y_2, Z_1 and Z_2 approach a stationary distribution. The length of a vector separating two nearby points is X , so that $\lambda_1 = \langle \dot{X}/X \rangle$. The area spanned by the two vectors is $\delta A \sim XX' \delta \varphi \sim X^2 \delta \varphi$, so that $\lambda_2 + \lambda_1 = \langle \delta \dot{\varphi}/\varphi \rangle + 2\langle \dot{X}/X \rangle$ (here we used the fact that $\delta \varphi \ll 1$).

We find the equations of motion for these variables. For X and $\delta \varphi$ we find $\dot{X} = Y_1 X/m$ and $\delta \dot{\varphi} = Z_2 \delta \varphi/m$, so that the Lyapunov exponents are

$$\lambda_1 = \langle Y_1 \rangle/m, \quad \lambda_2 = \lambda_1 + \langle Z_2 \rangle/m. \quad (8)$$

For θ , we find $\dot{\theta} = Y_2/m$, and conclude that θ executes a random walk, becoming uniform on $[0, 2\pi]$ as expected. For the remaining variables we find the following equations, where

$$\hat{\mathbf{n}}_1 = \hat{\mathbf{n}}_\theta, \hat{\mathbf{n}}_2 = \hat{\mathbf{n}}_{\theta+\pi/2}, F'_{ij}(t) = \hat{\mathbf{n}}_i \cdot \mathbf{F}(t) \hat{\mathbf{n}}_j$$

$$\begin{aligned} \dot{Y}_1 &= -\gamma Y_1 + (Y_2^2 - Y_1^2)/m + F'_{11} \\ \dot{Y}_2 &= -\gamma Y_2 - 2Y_1 Y_2/m + F'_{21} \\ \dot{Z}_1 &= -\gamma Z_1 - 2(Z_1 Z_2/2 + Y_1 Z_1 - Y_2 Z_2)/m + F'_{21} + F'_{12} \\ \dot{Z}_2 &= -\gamma Z_2 - 2(Z_2^2/2 + Y_1 Z_2 + Y_2 Z_1)/m - F'_{11} + F'_{22} . \end{aligned} \quad (9)$$

In the limit where the correlation time of the random velocity field is short, we can approximate eqns. (9) by a set of coupled Langevin equations. We write these in a dimensionless form by introducing dimensionless variables x_i , such that $(Y_1, Y_2, Z_1, Z_2) = m\gamma(x_1, x_2, x_3, x_4) \equiv m\gamma\mathbf{x}$, $t' = \gamma t$ and find

$$d\mathbf{x} = \mathbf{v}(\mathbf{x})dt' + d\mathbf{w} \quad (10)$$

where $v_1 = -x_1 + (x_2^2 - x_1^2)$, $v_2 = -x_2 - 2x_1 x_2$, $v_3 = -x_3 - x_3 x_4 - 2(x_1 x_3 - x_2 x_4)$, $v_4 = -x_4 - x_4^2 - 2(x_1 x_4 + x_2 x_3)$, $\langle dw_i \rangle = 0$, $\langle dw_i dw_j \rangle = 2D_{ij}dt'$. The diffusion matrix with elements D_{ij} is

$$\mathbf{D} = D_0 \begin{pmatrix} 1 & 0 & 0 & -(\Gamma+1)/2 \\ 0 & \Gamma & (\Gamma+1)/2 & 0 \\ 0 & (\Gamma+1)/2 & \Gamma+1 & 0 \\ -(\Gamma+1)/2 & 0 & 0 & \Gamma+1 \end{pmatrix} \quad (11)$$

where

$$D_0 = \frac{1}{2m^2\gamma^3} \int_{-\infty}^{\infty} dt \langle F_{11}(t)F_{11}(0) \rangle, \quad \Gamma = \frac{1+3\alpha^2}{3+\alpha^2}. \quad (12)$$

In our simulations, $D_0 = (3 + \alpha^2)\sigma^2/(2m^2\gamma^3\xi^2)$. The three parameters describing caustic formation are obtained from the stationary state of the Langevin process (10): the rate J at which a representative particle passes through a caustic is the same as the frequency with which the area of the parallelogram spanning the two vectors \mathbf{r} and \mathbf{r}' becomes equal to zero, or equivalently the rate at which $\delta\varphi$ passes through zero. An equivalent condition is that the trajectory in the (Z_1, Z_2) plane goes to infinity (reappearing from the reflected direction): $J = \gamma j$, where j is the rate at which x_4 escapes to infinity. Fig. 3(d) shows a comparison between a direct evaluation of the Lyapunov exponents (using a method described in [11]), and a simulation using eq. (10).

Eq. (10) is equivalent to a Fokker-Planck equation for the distribution $P(\mathbf{x}, t)$, namely $\partial P/\partial t' = \nabla \cdot [-\mathbf{v}P + \mathbf{D}\nabla P]$. Considering a steady-state solution in the limit $D_0 \rightarrow 0$, we find that a WKB ansatz, of the form $P(\mathbf{x}) = \exp[-\Phi(\mathbf{x})/D_0]$, is appropriate. We therefore expect that the escape current vanishes exponentially as $D_0 \rightarrow 0$, being of the form $j \sim j_0 \exp(-\Phi_0/D_0)$ (where j_0 may have an algebraic dependence on D_0). Fig. 3(e) shows that the caustic formation rate does vanish exponentially as $D_0 \rightarrow 0$, with action $\Phi_0 \approx 0.14$.

REFERENCES

- [1] G. L. Gooberman, *Ultrasonics: Theory and Application*, Hart Publications: New York, (1969).
- [2] R. A. Shaw, *Annu. Rev. Fluid Mech.*, **35**, 183, (2003).
- [3] M. Wilkinson and B. Mehlig, *Phys. Rev. E*, **68**, 040101, (2003).
- [4] B. Mehlig and M. Wilkinson, *Phys. Rev. Lett.*, **92**, 250602, (2004).
- [5] M. V. Berry, *Singularities in Waves*, Les Houches Lecture Series Session XXXV, eds. R. Balian, M. Kléman and J-P. Poirier, North Holland: Amsterdam, 453-543, (1981).
- [6] J. Deutsch, *J. Phys.*, **A18**, 1457, (1985).

- [7] M. A. Topinka, R. M. Westervelt, and E. J. Heller, *Physics Today*, Dec. 2003, p. 47.
- [8] L. Kaplan, *Phys. Rev. Lett.*, **89**, 184103, (2002).
- [9] H. Sigurgeirsson and A. M. Stuart, *Phys. Fluids*, **14**, 4352-61, (2002).
- [10] J. Bec, *Phys. Fluids*, **15**, L81-84, (2003).
- [11] J. P. Eckmann and D. Ruelle, *Rev. Mod. Phys.* **57**, 617-656, (1985).